Available online at www.sciencedirect.com

SciVerse ScienceDirect

Journal of the European Ceramic Society 32 (2012) 2203–2211

www.elsevier.com/locate/jeurceramsoc

Improving cutting quality by analysis of microstructure characteristics and solidification behaviour of recast layer formation on laser cut ceramic

Xiaochuan Chen, Lingfei Ji *, Yong Bao, Yijian Jiang

Institute of Laser Engineering, Beijing University of Technology, Beijing 100124, PR China

Received 20 January 2012; received in revised form 4 March 2012; accepted 12 March 2012
Available online 4 April 2012

Abstract

We studied the microstructure characteristics and solidification behaviour of the recast layer on a 1 mm Al_2O_3 electronic ceramic substrate processed by CO_2 laser cutting to improve the cutting quality. SEM (scanning electron microscope) and CLSM (confocal laser scanning microscope) observations showed that the upper and lower regions of the recast layer consist of equiaxed grains, while columnar grains dominate in the middle region, downgrading cutting quality. We used finite element modelling (FEM) to understand the solidification mechanism and explain profile and microstructure variation along the kerf. Using this analysis, we performed experiments to study the influences of assist gas pressure and laser cutting speed on the grain size and recast layer thickness. A thin, dense recast layer of uniform thickness and microstructure resulted from the following optimal parameters: 8 bar N_2 assist gas pressure, cutting speed of 1500 mm/min, and laser fluence of 200 W.

Keywords: Laser cutting; Grain size; Al_2O_3; Thermal conductivity; Substrates

1. Introduction

Compared to traditional mechanical ceramic cutting techniques, laser processing provides several advantages, such as high efficiency, low noise, and zero mechanical stress.[1–4] The demand for miniaturisation and high precision in the electronics industry drives the need for high quality cutting of hard and brittle electronic ceramics. High quality cutting also reduces final machining processes, thus lowering production costs. Dissimilar to thick ceramic laser cutting, crack elimination in thin ceramic laser cutting is a relatively mature research field, resulting in crack-free cutting of electronic ceramic substrates (∼1 mm thickness) by parameter optimisation.[5,6] Current research focuses more on improving cut surface quality. Our previous work shows that the laser cut recast layer on thick ceramic surfaces is easily detached because of loose microstructure.[7] However, the recast layer of laser cut thin ceramics is too consolidated for removal. Thus, to achieve high cutting quality for thin electronic ceramics, it is essential to obtain a thin, dense recast layer of uniform thickness and microstructure.

Current studies generally consider two aspects of improving cutting quality. One aspect is to improve cut surface roughness. Through analysis of mullite-alumina cross-sections, Quintero et al. showed that higher assist gas pressures reduce the recast layer extension along the beam direction.[8] Furthermore, lower laser frequency reduces the recast layer thickness and dross size. By investigating cut surface profiles, Li et al. improved cutting quality by period striation elimination on both metal and ceramic. The striation is removed as the continuous wave (CW) mode laser cutting speed increases, while lower assist gas pressures result in a wider operating window of cutting speeds.[9–11] For pulsed lasers, high peak power and high pulse repetition rate are necessary for evaporation to govern the cut process and stabilise cut front movement.[12]

Another aspect for improving cutting quality is to consider a numerical simulation analysis of the melt flow and temperature distribution along the cut surface. Schulz et al. used a variational formulation and finite dimensional approximation to develop a mathematical melt flow model. In particular, they adopted a 1D heat conduction model for melting front axial dynamics.[13] Ermolaev et al. established a mathematical model for oxygen laser cutting of mild steel. Here, a 3D temperature field and profile simulation predicted a temperature increase with downward melt flow.[14,15] Makashev et al. used a quantitative laser

* Corresponding author. Tel.: +86 10 67392052.
E-mail address: ncltji@bjut.edu.cn (L. Ji).

0955-2219/$ – see front matter © 2012 Elsevier Ltd. All rights reserved.
doi:10.1016/j.jeurceramsoc.2012.03.020

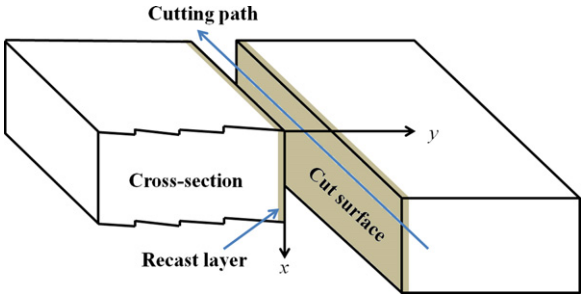

Fig. 1. Cross-sectional view of the work-piece.

cutting model for recast layer and dross generation.[16] Simplifications include, using a point heat source, rather than a surface heat source, and neglecting overheating and heat transfer across the thickness direction. Though simulation analysis can support experiment research, the latter simplifications make it difficult to provide direct guidance for laser processing optimisation. Currently, no satisfactory mathematical model exists for describing the complex rapid laser cutting process.[17]

Microstructural material features, including shape, size, orientation and grain arrangement, provide direct information about thermal or mechanical effects. It is therefore worthwhile to look at laser process optimisation based on an analysis of microstructural features of a laser-cut ceramic. In this paper, we study the temperature distribution and cooling effect variation along the kerf for processing optimising by analysing microstructure characteristics and solidification behaviour of recast layer. Our analysis shows the effect of assist gas pressure and cutting speed on recast layer formation, and results in a defect-free cut surface specimen with a uniform microstructure and thin recast layer.

2. Materials and methods

We used 96% alumina electronic ceramics with a thickness of 1 mm and a density of 3.77 g/cm^3. Because of good beam quality (TEM_{00}, $M^2 < 1.1$) and high absorption coefficient on Al_2O_3 (up to 80%), we employed a slab CO_2 laser (Rofin DC035) in CW mode, with 127 mm focal length lens; and a focused beam spot diameter of about 100 μm. The focal point position was 0.5 mm below the upper surface of the work-piece, with a standoff distance of 1 mm. The laser power was set to 200 W and cutting speeds ranged from 500 mm/min to 1500 mm/min. N_2, O_2 and compressed air were used as assist gases respectively for comparative experiment and N_2 was eventually selected for the experiments afterwards with gas pressure varied from 1 to 8 bar.

We used the work-piece for external profile cutting. Microstructure characteristics of a cross-sectional view of the cut surface recast layer (Fig. 1) were analysed using a scanning electron microscope (SEM, FEI Quanta 200) and confocal laser scanning microscope (CLSM, Olympus OLS 3000). The solidification process and assist gas velocity influence on the recast layer were studied using Ansys.

3. Results and discussion

3.1. Comparative experiment with difference assist gases

In metal laser cutting, N_2, O_2 and inert gas such as He and Ar are often used to be as assist gas for different processing application. However, in ceramic laser processing, no such preference is shown between the gases with different chemical properties because chemical reactions seldom take place due to the stable chemical properties of ceramics, even at high temperature condition. The difference processing effect induced by the assist gases is mainly the shear stress and cooling effect they provide. Variation of shear stress and cooling effect mainly attributes to the density, heat capacity, thermal conductivity and viscosity difference of gases. Due to a higher cost of He and Ar, comparative experiment was focused on N_2, O_2 and compressed air. The physical properties in temperature of 300 K and 100 kPa absolute pressure are shown in Table 1.

As demonstrated, the physical property difference amongst the assist gases is small which indicates that their effect on ceramic laser cutting should be similar. The similar experiment result with different assist gases coincided with the comparable physical properties of them. Fig. 2 is the CLSM images of the kerf vertical edge cross-section taken at the same position of the specimens, which were cut with different assist gases in 2 bar gas pressure and 1500 mm/min cutting speed. As marked in the images, a thin recast layer is attached firmly to the base material and there is no obvious boundary between the two regions, making it difficult to remove the recast layer. One can distinguish between the recast layer and the base material only by grain morphology differences as shown in Fig. 3, a high magnification SEM image of the cross-section: the base material consists

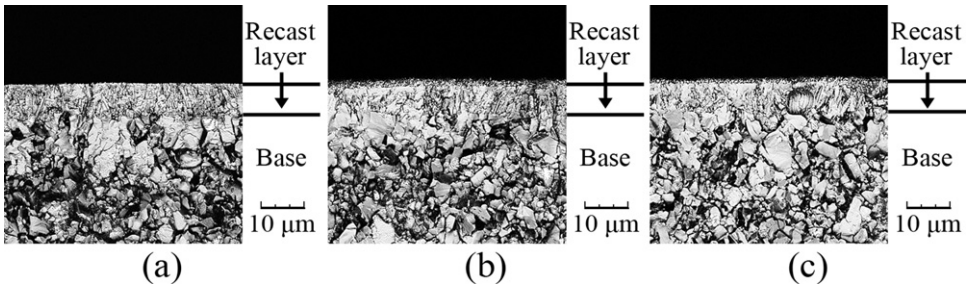

Fig. 2. CLSM images of work-piece cross-section cut with different assist gases: (a) N_2, (b) O_2 and (c) compressed air.

Table 1
Physical properties of N_2, O_2 and compressed air [18].

Type of assist gas	Density (kg/m^3)	Isobaric heat capacity (kJ/(kg K))	Thermal conductivity (mW/(m K))	Dynamic viscosity (μkg/(s m))
N_2	1.123	1.041	25.97	17.89
O_2	1.284	0.920	26.49	20.65
Compressed air	1.161	1.007	26.38	18.54

of equiaxed grains of about 5 μm in size, while recast layer structure is more compact with a much smaller grain diameter. On the other hand, the profile and microstructure of recast layer with different assist gases is similar. The thickness is 7.1–7.8 μm for all specimens shown in Fig. 2 and the recast layer consists of refined grains with diameter about 0.8 μm.

It can be concluded that the difference of the effect on the kerf quality of different assist gases employed in thin ceramic laser cutting is small. However, due to a lower ionisation potential of O_2, plasma would generate easily while using O_2 as assist gas in high laser power processing. Thus, O_2 was not used in the following experiment because plasma can attenuate laser energy absorbed by the work-piece and may eventually lead to cut failure. Besides, for concern of cost and component purity, compressed air was not selected as assist gas. Accordingly, N_2 was used for the following experiment to assist the cutting process.

3.2. Microstructure evolvement characteristics of recast layer

To study recast layer microstructure characteristics dependence on laser cutting parameters, we employed cross-section specimen cutting at a speed of 1200 mm/min and assist gas pressure of 4 bar for the SEM analysis. Fig. 4(a) is the kerf vertical edge SEM image showing the relative positions of Fig. 4(b)–(f). Based on morphology features, we divided the analysis region of the recast layer cross-section into three regions, namely the upper region (between the beam entrance edge and the middle of the kerf), the lower region (about 100 μm from the bottom (beam exit) edge), and the middle region (between the upper and lower regions).

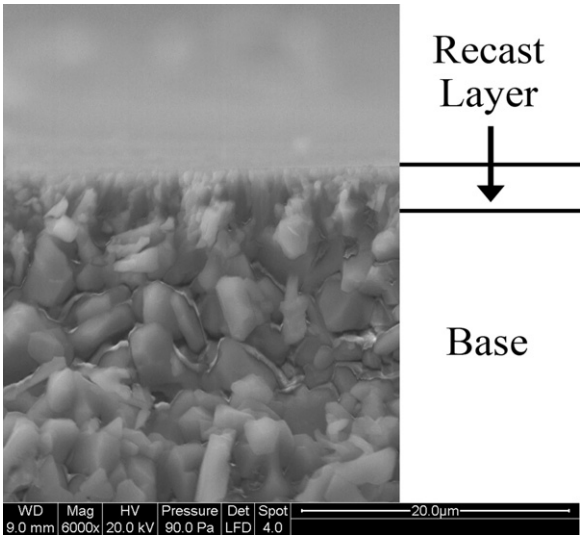

Fig. 3. SEM image of the work-piece cross-section.

Fig. 4(b) and (c) reveals a thin upper region recast layer. The layer consists of equiaxed grains much smaller than those in base material. The recast layer thickness increases in the upper region along the kerf from 3.4 to 6.3 μm. The thickness increases sharply in the middle region. The higher magnification SEM images in Fig. 4(d) and (e) shows that the dominant anisometric columnar grains in the middle region result in increasing recast layer thickness. The columnar grain growth direction is mainly perpendicular to the cut surface. The diameters and lengths are 0.5–0.7 μm and 5.6–9.6 μm, respectively, larger than the average grain sizes in the base material and upper region. On entering the lower region, the number and length of columnar grains decrease. Columnar grains are not observed while approaching the bottom edge (Fig. 4(f)). The recast layer thickness decreases to about 4 μm in the lower region and grain sizes are smaller than those in the base material.

3.3. Analysis of recast layer grain growth variation

In Fig. 4, we see that equiaxed grains emerge in the upper and lower regions, while columnar grains, with the growth direction perpendicular to the cut surface, dominate in the middle region. The variation of thickness and microstructure characteristics of the recast layer in different regions along the kerf vertical edge reflects altered solidification behaviour under different temperature conditions.

The formation of the columnar grains in the middle region leads to a thicker recast layer than in other regions. Recast layer structure defects and mismatch with the base material deteriorate with increasing recast layer thickness, resulting in an eventual unexpected break off from the cut surface. Hence, kerf quality can be improved by appropriate thickness reduction of the consolidated recast layer. On the other hand, the volume property of columnar grains makes brittle deformation more troublesome compared to equiaxed grains, because there are fewer plastic slip systems in the direction perpendicular to grains. In summary, there is an obvious dissimilarity of microstructure and thickness in the different regions of the recast layer, which deteriorates the cut surface quality. As a result, the columnar grain growth should be suppressed to obtain a thin and uniform recast layer.

Grain generation in ceramics follows the steps of nucleation and growth. After nucleation, grains grow as the solid–liquid boundary moves. Thornton reports that temperature differences

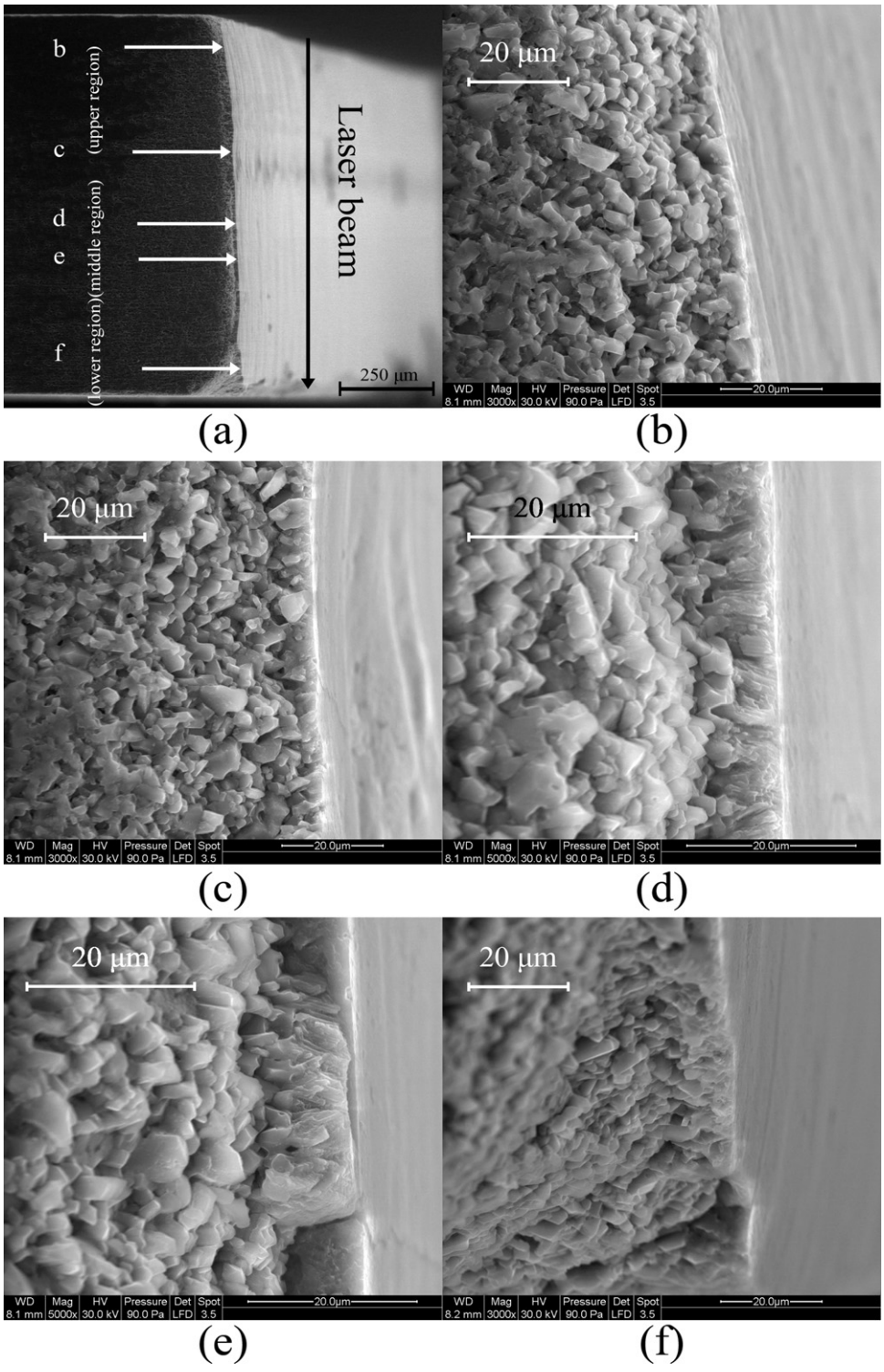

Fig. 4. SEM images of recast layer microstructure characteristics. (a) The work-piece cross-section and (b)–(f) higher magnification images of different regions along the kerf.

between the base and molten material causes microstructure variation after solidification.[19,20] In laser processing, the critical value for columnar grain generation is[21]:

$$\frac{G_T}{v_b} = \frac{\Delta T}{D}, \tag{1}$$

where G_T denotes the temperature gradient in the recast layer thickness direction, v_b represents moving velocity of the solid–liquid boundary, $\Delta T = T_l - T_s$ refers to the equilibrium freezing range, T_l and T_s denote the liquidus and solidus temperatures, respectively, and D is the liquid diffusion coefficient. Columnar grains emerge when the left side of Eq. (1) is less

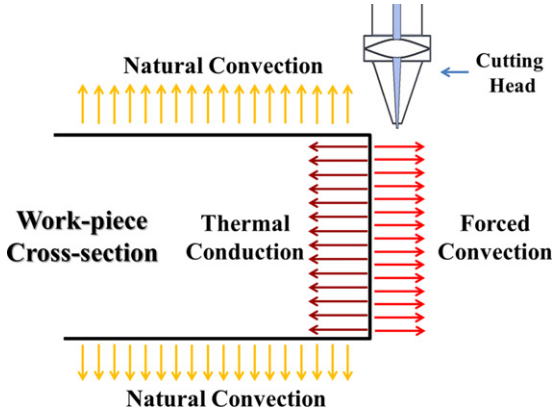

Fig. 5. Sketch of heat flux distribution during solidification.

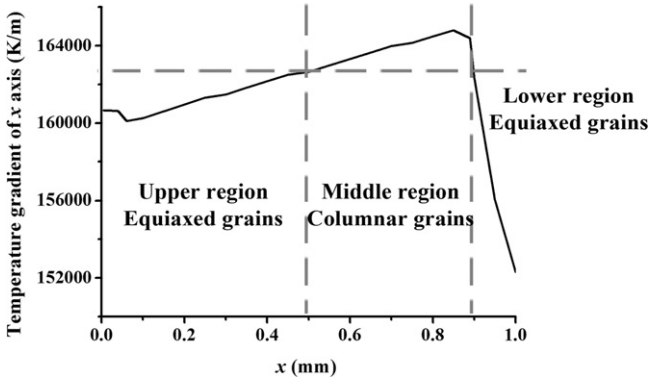

Fig. 6. Simulation result of transient temperature gradient along the kerf.

than the right side. Otherwise, equiaxed grains will be generated. Since the right side of Eq. (1) is constant, grain type formation depends on the temperature gradient and boundary velocity. As shown in Fig. 4, grain morphology variation along the kerf indicates a modified ratio of temperature gradient to boundary velocity. Compared to columnar grains in the middle region, the upper and lower regions indicate a higher ratio.

During solidification, there are three types of heat flux as shown in Fig. 5: forced convection of the molten material and assist gas, natural convection on the base material surface, and heat conduction from the molten material to the base. For analysing forced convection, the Reynolds number, Re, needed for characterising different flow regimes, is given by:

$$Re = \frac{ud}{\nu} = \frac{f(a)d}{\nu}\sqrt{\frac{2p}{\rho}}, \tag{2}$$

where d denotes the specimen thickness, ν is nitrogen kinematic viscosity, u is the kerf assist gas velocity calculated from Bernoulli's equation,[22] p is the gas pressure, ρ is the nitrogen density, and $\sqrt{2p/\rho}$ denotes the maximum gas velocity for a specific pressure. The value of $f(a)$ increases with kerf width a, with estimated $f(a)$ values (using simulations similar to those in Section 3.4) between 0.01 and 0.1, representing the cut surface effect on assist gas flow. The Reynolds number extracted from Eq. (2) is far less than the critical value 5×10^5, indicating laminar gas flow in the kerf. Hence, we calculated forced convection heat flux, q_1, from[23]:

$$q_1 = \frac{k\Delta T'}{d}Nu = \frac{0.664k\Delta T'\,Re^{1/2}\,Pr^{1/3}}{d}, \tag{3}$$

where k is the nitrogen thermal conductivity, $\Delta T'$ denotes the temperature difference between assist gas pressure and molten material, Nu refers to the assist gas Nusselt number, and Pr denotes a Prandtl number of 0.718 for nitrogen. For a temperature difference of 2200 K (based on the difference between room temperature and alumina melting point), and assuming independence of assist gas density and specific heat with temperature, we estimated the heat flux to be of order 10^6 W/m^2. We estimated natural convection heat flux, q_2, from:

$$q_2 = h\Delta T', \tag{4}$$

where h denotes a heat transfer coefficient of about 5–20 W/(m^2 K). The heat flux is of the order 10^4 W/m^2. We calculated heat conduction flux, q_3, from Fourier's law of heat conduction, namely:

$$q_3 = -\lambda \cdot gradT, \tag{5}$$

where λ refers to alumina conductivity of 24 W/(m K) for the material used in our experiment. Using recast layer thickness and temperature difference between boiling and melting points of alumina, we estimated a maximum temperature gradient of about 10^7 K/m, though the actual value may be much lower. Theoretically, the highest heat flux is of order 10^8 W/m^2, and decreases along the heat flux direction into the base.

Based on the above discussion, we used Ansys to perform a 2D numerical simulation. The thermal model includes natural convection, forced convection, and base material conduction. The simulation does not consider material melting and vaporisation. We applied a surface heat source based on the experiment to the cut surface. Assist gas pressure was set to 2 bar. The transient cut surface temperature gradient shown in Fig. 6 reflects the variation trend along the kerf. The temperature gradient increased in the upper and middle regions, and decreased sharply in the lower region.

The low thermal conductivity of alumina prevents rapid conduction of the energy absorbed in the upper region, resulting in a relatively low temperature gradient. As assist gas flowing along the kerf, the temperature of the assist gas increases because of forced convection with molten material. The temperature difference between molten material and assist gas is lower in the lower region compared to that in the upper and middle region, reducing forced convection heat flux according to Eq. (3). Therefore, the cooling effect in the lower region weakens, decreasing the temperature gradient.

Normally, columnar grain generation follows higher temperature gradients. Assuming the critical value for columnar grains formation is around 163,000 K/m in the transient simulation result obtained above, the curve was divided into three parts as shown in Fig. 6. The value in the middle part is above the critical value where columnar grains would generate, while in the left and right part of the curve, they would not emerge because the temperature gradient is below the critical value. The division of the curve agreed with the microstructure variation of the

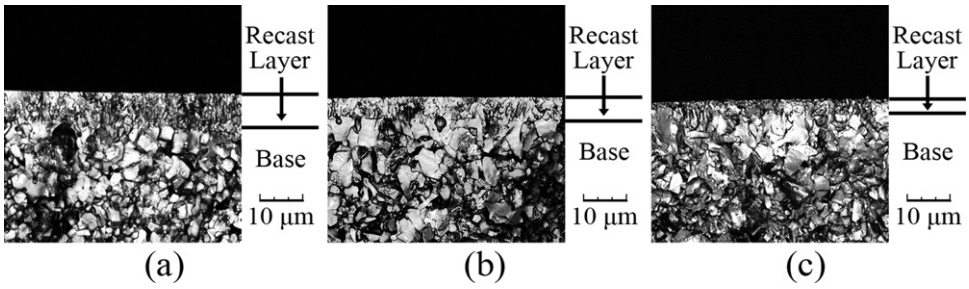

Fig. 7. CLSM images of the work-piece cross-section for different assist gas pressures p: (a) $p = 2$ bar, (b) $p = 5$ bar and (c) $p = 8$ bar.

kerf recast layer demonstrated in Fig. 4. On the other hand, the boundary velocity in Eq. (1) is also known as cooling rate.[21] As already mentioned, three types of heat flux exist during the solidification process of the recast layer. Cooling through the upper surface of the upper region can only occur by natural convection. However, numerical analyses of Eqs. (3)–(5) show natural convection cooling is inefficient compared to forced convection and conduction. The same situation occurs for cooling from the lower region of the lower surface of the work-piece. Because of the lack of base material surface, natural convection does not occur in the middle region of the kerf. Heat transfer takes place by forced convection and thermal conduction along the $\pm y$ axis direction; this is more efficient than natural convection. Hence, a much higher cooling rate is achieved in the middle region, leading to a lower ratio of temperature gradient to boundary velocity and columnar grain formation according to Eq. (1). Consequently, because of a much lower cooling rate and thus higher ratio, equiaxed grains generate in the upper and lower regions. The above analysis and simulation results agree with microstructure variation of the recast layer.

For laser processing, one can control the temperature variation by optimising parameters such as laser power, assist gas pressure and cutting speed. Normally, we need to exceed a critical power density value to achieve a successful cut kerf through melt removal and/or evaporation. In a pre-research experiment, for a fixed focal point position, we obtained a kerf with laser power of 200 W. Fixing the laser power at 200 W, the following discussion focuses on assist gas pressure and cutting speed parameters.

3.4. Effect of assist gas on solidification behaviour

For fixed laser energy input and cutting speed, assist gas pressure plays a vital role in the temperature variation inside the kerf. We chose the following parameters: 200 W laser power, 1000 mm/min cutting speed, and 2, 5, 8 bar assist gas pressures. Fig. 7 shows CLSM images taken at the same position (about 200 μm above the bottom edge) for different specimens: and it shows that the recast layer thickness decreases with increasing assist gas pressure. For 2 bar assist gas pressure, the thickness is 6.5–8.0 μm (Fig. 7(a)), decreasing to 4.6–5.4 μm for 5 bar pressure (Fig. 7(b)), and further decreasing to 3.2–4.0 μm for 8 bar pressure (Fig. 7(c)). At the same time, columnar grains were well restrained with assist gas pressure increase.

The assist gas pressure affects cooling and wall shear stress. According to Eqs. (2) and (3), higher assist gas pressures result in higher forced convection heat flux, leading to better cooling effects for grain refinement, thus improving recast layer density and uniformity. More importantly, higher assist gas pressures increase wall shear stress. In the work on boundary layers,[24] Blasius assesses wall shear stress, τ_w, by:

$$\tau_w = 0.332u^{3/2}\sqrt{\frac{\mu\rho}{x}} = 0.332\, f(a)^{3/2}\sqrt[4]{\frac{(2p)^3\mu^2}{\rho x^2}}, \tag{6}$$

where μ is the dynamic viscosity of the melt layer, and x denotes the kerf position x-axis coordinate (see Fig. 1). Because the change in condition of a through cut was small, we considered ρ to be constant. As the assist gas pressure p increases, the melt layer surface temperature decreases and, consequently, μ increases. We neglected the effect of p on kerf width, and thus also neglected $f(a)$. Hence, for a fixed position x, τ_w increases with increasing assist gas velocity in the kerf, thus achieving a higher wall shear stress by increasing the assist gas pressure. The increasing shear stress applied to the melt layer, leads to a growing melt removal rate for recast layer thinning under high gas pressure.

To validate the effect of assist gas on recast layer thickness, we developed a numerical simulation for a typical sample: we set the assist gas pressure to 2 bar, and chose kerf profile (Fig. 8) widths, 130 μm and 120 μm, at the top and at the outlet, respectively.

Fig. 9 shows the simulation result, which describes the velocity field of assist gas along the x axis ($-y$ axis in the Ansys

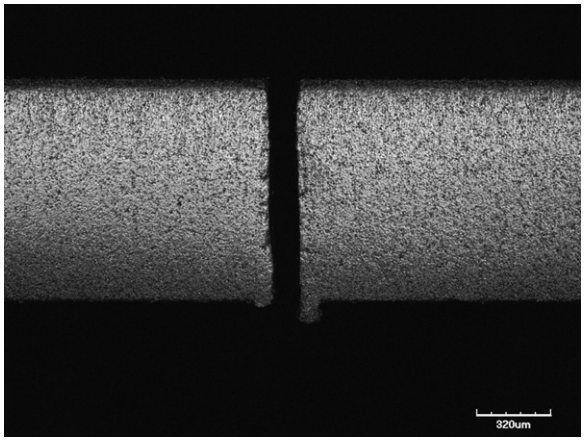

Fig. 8. Typical CLSM kerf profile for 2 bar assist gas pressure.

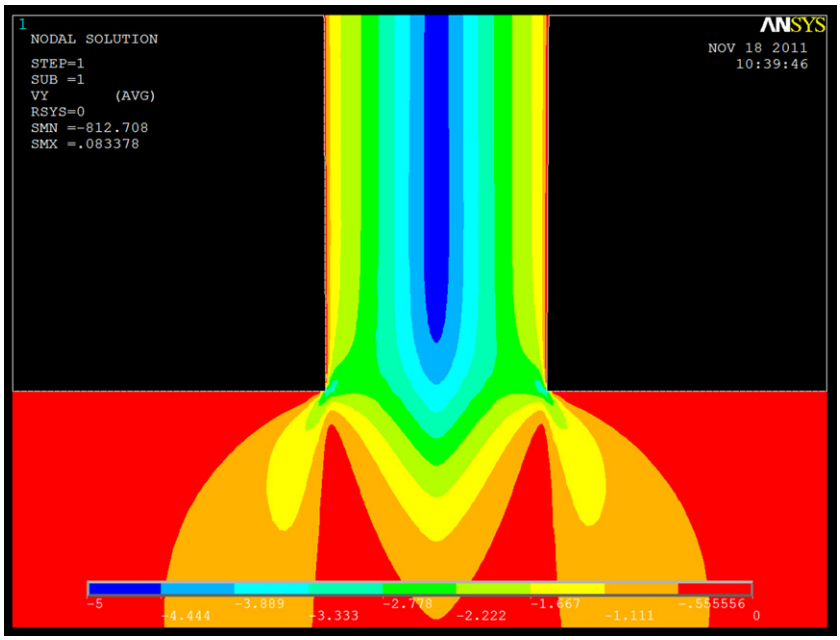

Fig. 9. Simulation contour map of assist gas velocity along the *x* axis.

coordinate system) near the kerf outlet. The black region in Fig. 9 represents the base material. Wall shear stress is defined as being proportional to the velocity gradient perpendicular to the surface, namely:

$$\tau_w = \mu \frac{\partial u(y)}{\partial y}\bigg|_{y=0}. \tag{7}$$

We see that the lower velocity region becomes smaller while approaching the kerf's bottom edge, i.e. the velocity gradient increases, resulting in increasing wall shear stress and thinner recast layer thickness as shown in Fig. 4(f). The velocity gradient variation is caused by a sharp increase of the assist gas flowing channel near the kerf outlet. For higher assist gas pressures, the velocity gradient increases because of a higher velocity reached in the kerf. Therefore, wall shear stress increases and the recast layer thickness decreases. Our simulation result supports the recast layer thickness dependence on assist gas pressure. Hence, we can reduce the recast layer thickness by controlling assist gas pressure. On the other hand, increasing assist gas pressure induced the cooling effect to rise, which resulted in a lower ratio of temperature gradient to boundary velocity according to Eq. (1). Therefore, the growth of columnar grains was suppressed. In summary, a higher assist gas pressure (~8 bar) removes excessive molten material and restrains the growth of columnar grains, yielding a thin and compact recast layer.

3.5. Effect of cutting speed on solidification behaviour

During ceramic laser cutting, altering the cutting speed adjusts energy input for fixed laser power, duty cycle and spot size. We examined specimens with the following cutting parameters: 200 W laser power, 2 bar assist gas pressure, and different cutting speeds of 500 mm/min, 1000 mm/min and 1500 mm/min. Fig. 10 displays CLSM images of the cross-section recast layer.

We can see that the thickness decreases with increasing cutting speed. For a cutting speed of 500 mm/min, the recast layer thickness is about 6.7–8.5 μm (Fig. 10(a)), and decreases to about 6.0–8.0 μm at a cutting speed of 1000 mm/min (Fig. 10(b)). For a cutting speed of 1500 mm/min, the thickness further decreases to about 5.5–6.0 μm (Fig. 10(c)). This indicates a higher melt removal rate caused by cutting speed variation, though the extent is smaller compared to the effect of assist gas pressure. On the other hand, Fig. 10 shows an obvious decrease in columnar grain diameters with increasing cutting speed: the diameter decreases from 1.0–1.4 μm to 0.5–0.8 μm.

Because of cutting speed increase, the laser energy absorbed per input point decreases proportionally under constant laser fluence. For the same gas pressure (2 bar N_2), the heating time, at a certain input point induced by the laser energy absorption, reduces with increasing cutting speed. Consequently, a faster cooling process takes place, resulting in grain refinement, thus improving recast layer quality. Compared to assist gas pressure application for reducing the recast layer thickness, cutting speed plays a more important role for grain size refining. Hence, to obtain a dense recast layer with refined grains, we need to employ higher cutting speeds.

3.6. Optimised cutting result

In summary, to obtain a thin recast layer without columnar grains, we need to employ high assist gas pressure and cutting speed, providing a high melt removal rate to reduce the recast layer thickness and refining the grains to achieve a dense, consolidated layer attached to the base material.

Fig. 11 shows the SEM images of recast layer cross-section with optimised cutting parameters of 1500 mm/min cutting

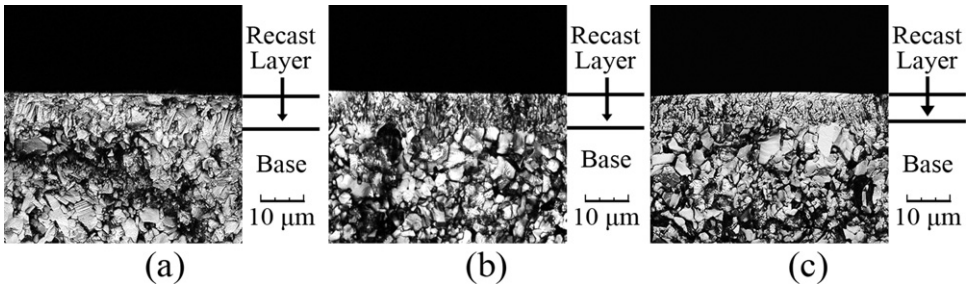

Fig. 10. CLSM images of work-piece cross-section for different cutting speeds u_c: (a) $u_c = 500$ mm/min, (b) $u_c = 1000$ mm/min and (c) $u_c = 1500$ mm/min.

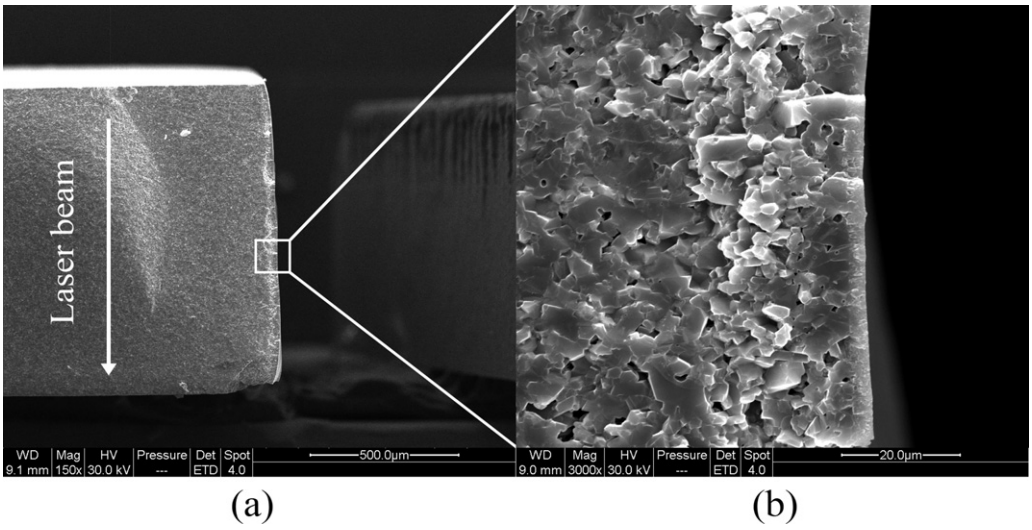

Fig. 11. SEM images of recast layer microstructure, showing (a) the work-piece cross-section and (b) a close-up view of (a).

speed, and 8 bar assist gas pressure. Fig. 11(b) displays a higher magnification SEM image of the recast layer microstructure in the middle region shown in Fig. 11(a). The recast layer thickness of 3.0–3.7 μm is consistent along the kerf. We do not observe the columnar grains which dominated the middle region in other specimens. The recast layer is firmly attached to the base material and the boundary is more distinct compared to the middle region shown in Fig. 4. Hence, we obtained a smooth cut surface of a uniform recast layer with refined grains.

4. Conclusions

Through analysis of microstructure and solidification behaviour of the work-piece, we improved the CO_2 laser cutting quality of alumina electronic ceramic with 1 mm thickness. Normally, the recast layer thickness increases from the upper to the middle region, and decreases in the lower region. Equiaxed grains dominate in the upper and lower regions, while massive columnar grains emerge in the middle region. Microstructure variation of the recast layer reveals temperature and solidification behaviour differences along the kerf. Our numerical simulation demonstrates that the x axis temperature gradient increases from the upper to the middle region, and decreases sharply in the lower region. Because of different solidification processes, the cooling rate in the middle region is higher than the upper and lower regions. Based on an analysis of the molten material solidification mechanism, we performed an experiment to study the relationship between laser cutting parameters and the recast layer profile. We observed that the recast layer thickness is mainly influenced by assist gas pressure, while cutting speed significantly affects grain refinement. To achieve a thin recast layer without columnar grains requires a higher assist gas pressure and cutting speed. We established the following optimal cutting parameters for obtaining high quality specimens: laser power of 200 W, 1500 mm/min cutting speed, and 8 bar assist gas pressure.

Acknowledgements

The authors acknowledge support from the National Natural Science Foundation of China (50875006), Program for New Century Excellent Talents in University (NCET-10-0007), and Beijing Natural Science Foundation (3111002).

References

1. Pascual-Cosp J, Ramírez del Valle AJ, García-Fortea J, Sánchez-Soto PJ. Laser cutting of high-vitrified ceramic materials: development of a method using a Nd:YAG laser to avoid catastrophic breakdown. *Mater Lett* 2002;**55**(4):274–80.
2. Quintero F, Pou J, Lusquiños F, Boutinguiza M, Soto R, Pérez-Amor M. Comparative study of the influence of the gas injection system on the

Nd:yttrium-aluminum-garnet laser cutting of advanced oxide ceramics. *Rev Sci Instrum* 2003;**74**(9):4199–205.
3. Samant AN, Dahotre NB. Laser machining of structural ceramics—a review. *J Eur Ceram Soc* 2009;**29**(6):969–93.
4. Yan Y, Li L, Sezer K, Wang W, Whitehead D, Ji L, et al. CO_2 laser underwater machining of deep cavities in alumina. *J Eur Ceram Soc* 2011;**31**: 2793–807.
5. Yan Y, Ji L, Bao Y, Jiang Y. Theory analysis and experiment verification on crack characters during laser processing ceramic. *Chin J Lasers* 2008;**35**(9):1401–8.
6. Lu G, Siores E, Wang B. An empirical equation for crack formation in the laser cutting of ceramic plates. *J Mater Process Technol* 1999;**88**:154–8.
7. Ji L, Yan Y, Bao Y, Jiang Y. Crack-free cutting of thick and dense ceramics with CO_2 laser by single-pass process. *Opt Laser Eng* 2008;**46**(10): 785–90.
8. Quintero F, Pou J, Lusquiños F, Boutinguiza M, Soto R, Pérez-Amor M. Quantitative evaluation of the quality of the cuts performed on mullite-alumina by Nd:YAG laser. *Opt Laser Eng* 2004;**42**(3):327–40.
9. Sobih M, Crouse PL, Li L. Elimination of striation in laser cutting of mild steel. *J Phys D: Appl Phys* 2007;**40**(22):6908–16.
10. Li L, Sobih M, Crouse PL. Striation-free laser cutting of mild steel sheets. *Annu CIRP* 2007;**56**(1):193–6.
11. Wee LM, Crouse PL, Li L. A statistical analysis of striation formation during laser cutting of ceramics. *Int J Adv Manuf Technol* 2008;**36**(7–8): 699–706.
12. Yan Y, Li L, Sezer K, Whitehead D, Ji L, Bao Y, et al. Nano-second pulsed DPSS Nd:YAG laser striation-free cutting of alumina sheets. *Int J Mach Tool Manu* 2012;**53**(1):15–26.
13. Schulz W, Kostrykin V, Niessen M, Michet J, Petring D, Kreutz EW, et al. Dynamics of ripple formation and melt flow in laser beam cutting. *J Phys D: Appl Phys* 1999;**32**(11):1219–28.
14. Ermolaev GV, Kovalev OB. Simulation of surface profile formation in oxygen laser cutting of mild steel due to combustion cycles. *J Phys D: Appl Phys* 2009;**42**(18):1–10.
15. Ermolaev GV, Kovalev OB, Orishich AM, Fomin VM. Mathematical modelling of striation formation in oxygen laser cutting of mild steel. *J Phys D: Appl Phys* 2004;**39**(19):4236–44.
16. Makashev NK, Asmolov ES, Blinkov VV, Burmistrov AY, Buzykin OG, Makarov VA. Gas-hydrodynamics of CW laser cutting of metals in inert gas. *Proc SPIE* 1994;**2257**:2–9.
17. Kovalev OB, Yudin PV, Zaitsev AV. Modeling of flow separation of assist gas as applied to laser cutting of thick sheet metal. *Appl Math Model* 2009;**33**(9):3730–45.
18. Haynes WM. *CRC handbook of chemistry and physics*. 91st ed. Boca Raton: CRC Press; 2010.
19. Thornton JA. High rate thick film growth. *Annu Rev Mater Sci* 1977;**7**:239–60.
20. Mazor A, Srolovitz DJ, Hagan PS, Bukiet BG. Columnar growth in thin films. *Phys Rev Lett* 1988;**60**(5):424–7.
21. Kannatey-Asibu Jr E. *Principles of laser materials processing*. New Jersey: Wiley; 2009.
22. Wandera C, Kujanpaa V. Characterization of the melt removal rate in laser cutting of thick-section stainless steel. *J Laser Appl* 2010;**22**(2):62–70.
23. Çengel YA, Ghajar AJ. *Heat and mass transfer: Fundamentals and applications*. 3rd ed. New York: McGraw-Hill; 2007.
24. Wiley-VCH. *Ullmann's modeling and simulation*. Weinheim: Wiley; 2007.